https://doi.org/10.1016/j.compstruct.2022.116434
This is the Pre-Published Version.

Novel slow-sound lattice absorbers based on the sonic black hole

Jun Wei Chua[a], Xinwei Li[a], Xiang Yu[b]* Wei Zhai[a,]*
[a] *Department of Mechanical Engineering, National University of Singapore, Singapore 117575*
[b] *Department of Mechanical Engineering, The Hong Kong Polytechnic University, Hong Kong SAR, 999077*

* Corresponding author.
E-mail address: lucien.yu@polyu.edu.hk, mpezwei@nus.edu.sg

Abstract

The advent of additive manufacturing enabled rapid progress in the research of lattice structures, such as truss lattices, for sound absorption applications. Thus far, the sound absorption coefficient curves of truss lattices are typically characterized by alternating regions of high and low coefficients, reminiscent to that of Helmholtz resonators. The relatively poor sound absorption performances of such lattices prompt a need for an alternative sound absorption mechanism to improve their performances. In this work, we propose to incorporate a series of thin parallel plates with circular holes resembling the profile of a sonic black hole (SBH) into truss lattices for the design of a novel class of slow-sound lattice absorbers (SSLA). Four truss lattices, based on the mimicry of Bravais lattices, are considered. Samples were manufactured using stereolithography and the sound absorption properties were measured using an impedance tube. A significant increase in the sound absorption coefficients throughout a broadband frequency range from 1000 to 6300 Hz was observed with the addition of SBH plates. Finite element modelling reveals that the SSLA exhibits both the frequency-dependent resonant cell mechanisms of the lattice absorber and the time-dependent sound speed retardation effects of the SBH. Compression tests also reveal significant improvements to the specific energy absorption and absorption efficiency for some of the structures. Overall, this work demonstrates the potential and a conceptual advance with the adoption of additional plates to induce the sound speed reduction mechanism in the design of sound-absorbing lattices.

Graphical Abstract

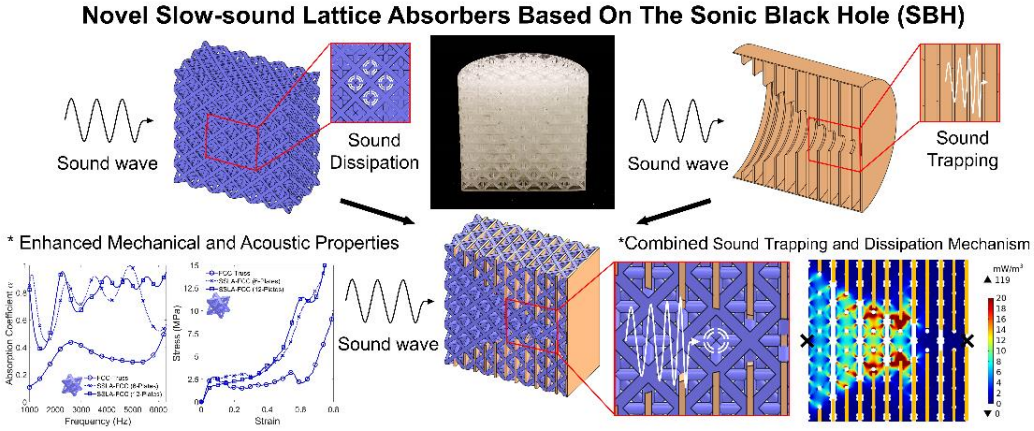

Highlights

- The work presents a slow-sound lattice sound absorber with sonic black hole plates.
- Samples were printed successfully using the vat photopolymerization technique.
- Sound absorption performances of the proposed lattices outweigh the truss lattices.
- The proposed lattices exhibit both resonance and sound speed reduction mechanisms.

© 2022 . This manuscript version is made available under the CC-BY-NC-ND 4.0 license https://creativecommons.org/licenses/by-nc-nd/4.0/.

Keywords
Lattice Structures, Acoustic Black Hole, Sound Absorption, Finite Element Modelling.

1. Introduction

With rapid urbanization and transport development, noise pollution and control have become one of the most important engineering challenges in the world today. Prolonged exposure to excessive noise can lead to serious health issues such as irreversible hearing loss, fatigue, stress, hypertension, coronary heart diseases, as well as cognitive impairment, especially in children [1]. To address this challenge, sound-absorbing materials are widely utilized. Many types of sound absorbers exist, such as foams and fibrous absorbers [2, 3], perforated panels [4-6] and structure-based acoustic metamaterials [7, 8]. Recently, there is an increasing demand for highly effective and customisable sound-absorbing structures which are more aligned with the operating requirements of existing structures [9, 10]. With the improvements in additive manufacturing (AM) technologies, designing such sound absorbers becomes much easier and more physics-driven.

In particular, one class of porous sound-absorbing materials made possible to manufacture using AM comes in the form of lattices, which are periodic and repeating 3D structured unit cells with struts, voids or plates within [11]. One of the more important classes of lattices is truss lattices, which are based on pre-determined spatial arrangements of struts in three-dimensional space [12]. Prior research on lattices shows that the capabilities allow them to perform various major functionalities, such as for lightweight applications [13-15], energy and impact absorbers [16-19], bio-implants [20], and materials with meta-behaviours [21]. In particular, there is an increasing interest in the study of truss lattices as sound absorbers, due to their vast network of open interconnecting pores and high degrees of design freedoms. Some of the previously studied lattice sound absorbers include various object-mimicking truss structures [22-25], triply periodic minimal surface (TPMS) structures [26] and spherical-cavity [27, 28] lattices. For the case of truss lattices, some key sound absorption characteristics include alternating frequency bands of high and low sound absorption with absorption peaks reminiscent of the Helmholtz resonance phenomenon [22, 23, 29]. These lattices can achieve high absorption coefficients approaching one at certain frequencies. However, the averaged sound absorption performances of such lattices are notably poor or have limited bandwidth [22, 23]. The sound absorption performance of a body-centred cubic (BCC) truss was studied recently [23]. Absorption coefficients are found to generally fall below 0.5 for many frequencies, even for samples of 40 mm length, while the peak absorption coefficients rarely exceed 0.7. In a work on multi-functional strut and plate lattices by Li et al. [22], a correlation between the number of lattice layers and the number of resonant peaks was observed, with the sound absorption coefficients being close to 1 for such peaks. However, the sound absorption coefficients were mostly below 0.5 elsewhere. These studies highlight a need for an alternative sound absorption mechanism that can complement the resonance-like effects in truss lattices in order to improve the overall sound absorption performances, while maintaining excellent mechanical properties necessary for practical applications.

A recently discovered approach to sound absorption comes in the form of the sonic black hole (SBH). The original concept of Acoustic Black Hole (ABH) was coined by Mironov [30], who studied the propagation of flexural waves in a beam whose thickness decreases smoothly to zero in a finite interval. It was shown that the velocity of flexural waves decreases with decreasing thickness, such that the incoming wave will gradually slow down and never reach the tip with a perfectly vanishing termination. The flexural waves tend to be trapped at the tip which in turn amplifies the vibration. To dissipate the concentrated vibration energy, a viscoelastic layer is usually introduced at the end of the beam to realize a non-reflecting boundary [31, 32]. Comparatively, SBH is proposed as the counterpart of structural ABH to

absorb sound waves in air [33]. It typically consists of a duct structure with decaying inner radii, where a set of rigid rings are added to provide a smoothly varying impedance boundary. The damping mechanism of such geometry involves the excitation of air molecules between adjacent parallel plates, causing significant viscous effects [34]. Theoretical analyses have shown that incoming sound waves will slow down progressively in the SBH structure, resulting in significant energy concentration. To absorb the focalized sound energy, an efficient damping mechanism is required to complete the SBH effect [8, 35, 36]. However, such couplings between the dissipative mechanism and the metamaterial behaviour of the SBH are not well understood with few research works in the literature [37]. Furthermore, although theoretical studies allude to promising wave manipulation ability, implementation of SBH absorber to consider material and fabrication process is less exploited, hampering its uses for noise control applications [31].

In this work, we report a novel class of slow-sound lattice sound absorbers (SSLA) with superior sound absorption and mechanical properties. These lattices were made by incorporating a set of parallel plates with a profile resembling the SBH into the design of truss lattices. Sound absorption measurements indicated a vast improvement in sound absorption coefficient as compared to pure truss lattices, with an average absorption coefficient of 0.72. Numerical simulations revealed that the mechanism of sound absorption for the lattices is a combination of viscous and thermal losses inherent in truss lattices, coupled with the slowing of sound propagation speeds and trapping of acoustic energy due to the geometry of the SBH plates. Quasi-static compression tests conducted on the lattices indicated improvements in compressive strengths, more uniform stress plateau, as well as an improvement in absorption efficiency and specific energy absorption for some of these lattices. This marks one of the first studies [37] that aims to leverage the utility of the sound deceleration effects due to the SBH structure into the lattice structure for the development of a novel class of high performing material.

2. Design Principles

An overview of the design strategy in this work is illustrated in Figure 1. The SSLA is constructed by incorporating an SBH structure into the truss lattice in the form of thin parallel plates, with the circular holes and the decaying inner radii mimicking an SBH profile. As mentioned in the introduction, previous sound absorption studies on truss lattices based on the mimicry of Bravais lattice structures have low average sound absorption coefficients and limited bandwidth. This motivates a search for an alternative sound manipulation mechanism that can complement the sound dissipation properties of truss lattices, preferably by focusing acoustic energy inside the absorber. Furthermore, while previous works on the SBH [8, 30] theoretically pointed out that sound waves can be gradually slowed-down in a tapered duct, an energy dissipation mechanism is necessary to tackle the focalized sound energy for the SBH to behave as an efficient sound absorber.

In this work, we embrace the SBH-induced slow-sound effect and the inherent viscous-thermal loss in the truss lattice to design a novel class of slow-sound lattice absorbers. The proposed lattice would be able to combine both sound speed reduction and energy focusing effect induced by the SBH plates, and frictional energy dissipation by the truss lattice part, respectively. The potential benefits of such composition are two-fold: First, the retardation of sound speed due to the SBH effect means that the period in which the waves propagate through the structure is increased. From the point of view of the incoming waves, it can also mean propagation through a duct with a longer effective length, which generally increases sound absorption. Second, owing to the slow-sound effect, sound speed is equivalently reduced, which means that the resonance frequency of the lattice absorber can be further shifted down. This proposed structure can then absorb a larger proportion of energy at lower frequencies.

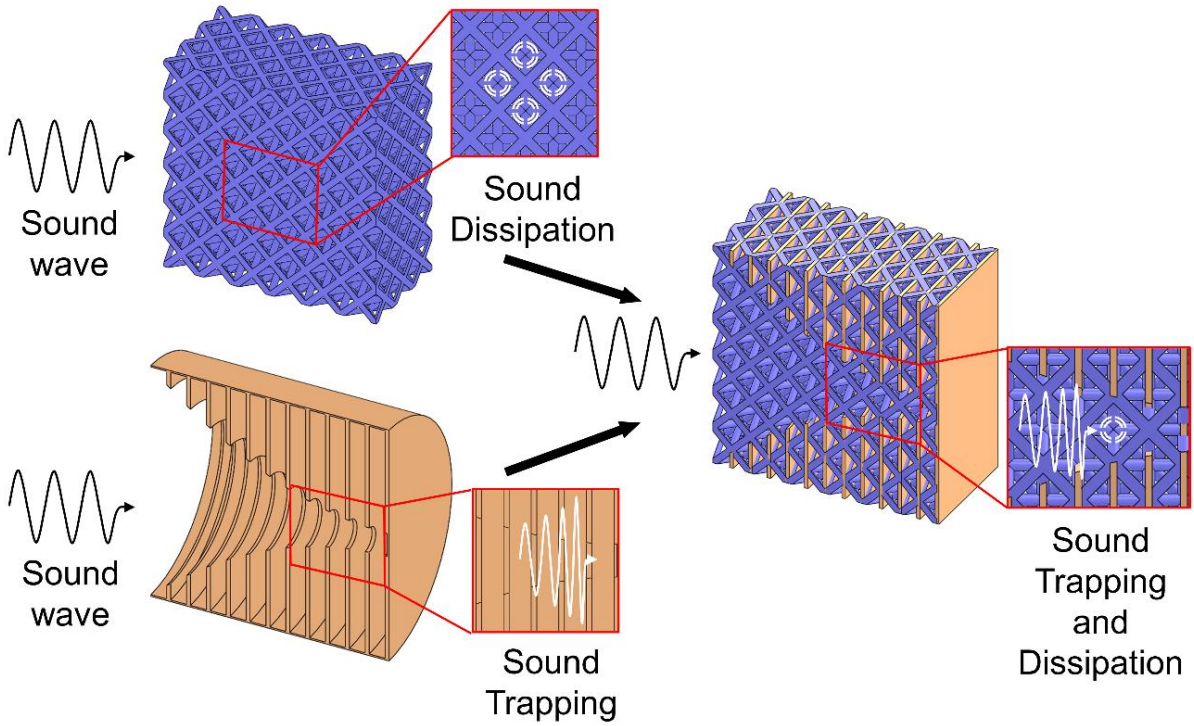

Figure 1: Overview of design strategy of the slow-sound lattice sound absorber (SSLA).

2.1. Lattice Design

Here, we focus on strut lattices based on the mimic of Bravais lattice structures. The orientation and arrangements of these types of lattices present several fundamental features of lattice designs, including horizontal, vertical, inclined, and constrained inclined strut members, which are then expected to lay technical grounds for understandings of SBH and lattice hybrids. The truss lattices to be used in this work are shown in Figure 2. These lattices are designed based on the simple cubic (SC), body-centred cubic (BCC), face-centred cubic (FCC) and fluorite crystal structures. Each strut added into the designs connects any two lattice points. The cell length is fixed to 5 mm while the strut diameters are chosen such that the relative density of the truss lattices is fixed at 30%, as labelled in each lattice in Figure 2.

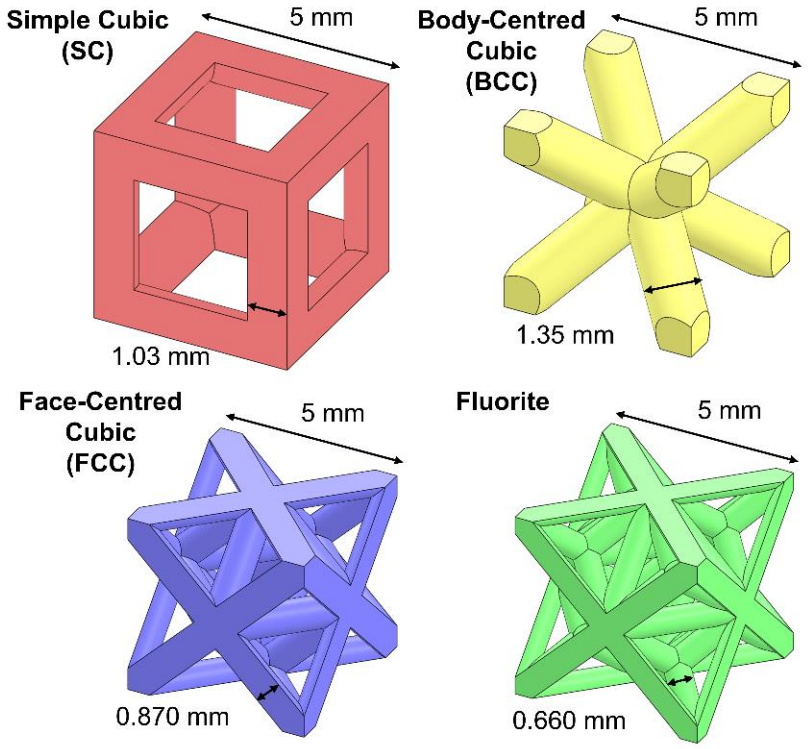

Figure 2: (a) Truss lattices considered in this work: (a) SC-Truss, (b) BCC-Truss, (c) FCC-Truss, (d) Fluorite-Truss. Important dimensions for the lattices were indicated.

2.2. SBH Design

The SBH is a novel sound manipulation concept in which incident sound waves enter a circular duct with annular rings with decreasing inner radius. An illustration of the SBH duct with important design parameters is shown in Figure 3. Based on the pioneering work by Mironov [33], the governing equation of sound propagation in the SBH structure is as follows,

$$\frac{\partial^2 p}{\partial x^2} + \frac{\partial p}{\partial x}\frac{\partial}{\partial x}(\ln S(x)) + p\left(k_0^2 + j\rho_0\omega\frac{2Y(x)}{h(x)}\right) = 0, \tag{1}$$

where p is the acoustic pressure, $\omega = 2\pi f$ is the angular frequency, f is the sound frequency, $k_0 = \frac{\omega}{c_0}$ is the wavenumber, ρ_0 is the density of air, c_0 is the speed of sound in air, and $h(x)$ and $S(x)$ are the radius and cross-sectional area of the duct at position x respectively. The wall admittance, $Y(x)$, for circular ducts is given by [8]

$$Y(x) = -\frac{j\omega}{\rho_0 c_0^2}\frac{R^2 - h^2(x)}{2h(x)}. \tag{2}$$

For an SBH with a quadratically decaying profile, its inner radius takes the following form:

$$h(x) = \frac{R}{L^2}x^2, \tag{3}$$

where *R* is the radii of the circular duct at the entrance and *L* is the length of the duct, it was found that the phase and group velocities of sound wave propagation were solved by Mironov [33] as follows,

$$c_{ph} = \frac{\omega}{k} = -\frac{\omega}{\sqrt{k_0^2 L^2 - 1}}x; \tag{4}$$

$$c_g = -\frac{c_0^2\sqrt{k_0^2 L^2 - 1}}{L^2\omega}x. \tag{5}$$

It can then be seen that $\lim_{x\to 0^-} c_{ph} = 0$ and $\lim_{x\to 0^-} c_g = 0$, which implies that both the phase and group velocities tend to zero near the termination. Under this circumstance, the sound wave will not reach the termination and be reflected, resulting in sound energy being focused inside the duct without any reflection of transmission.

For a more general case where the termination radius of the duct r tends towards a finite value, the SBH profile takes the form

$$h(x) = \frac{R-r}{L^2}x^2 + r. \tag{6}$$

Based on the works by Mi et al. [8], the phase and group velocities of sound wave propagation are as follows,

$$c_{ph} = \frac{\omega}{k} = \frac{\omega[(R-r)x^2 + rL^2]}{\sqrt{k_0^2R^2L^4 - 4(R-r)^2x^2}}; \tag{7}$$

$$c_g = \frac{c_0^2[(R-r)x^2 + rL^2]\sqrt{k_0^2R^2L^4 - 4(R-r)^2x^2}}{\omega L^4R^2}. \tag{8}$$

Note that $\lim_{x\to 0^-} c_{ph} = \frac{r}{R}c_0$ and $\lim_{x\to 0^-} c_g = \frac{r}{R}c_0$, which implies that the phase and group velocities decrease to a finite value. If the ratio of R/r is large, such a decrease in sound speed is sufficient to increase the travelling time for any sound wave to remain in the truss-SBH lattice, which can help to enhance the sound absorption performance of the SSLA. The parameters that may influence the sound absorption capabilities of the SBH include the length of duct L, the SBH profile of the acoustic duct $h(x)$, the diameter of the duct at the entrance R, the inner diameter of the duct at the termination r, number of rings utilised to replicate the thickness profile, thickness of each ring t and damping mechanisms to be used. Specific values of the parameters used in the work are appended in Table 1. Note that this work considers two numbers of plates, each representing cases when the cavity between adjacent plates is filled by one or half of the unit cells in Section 2.1.

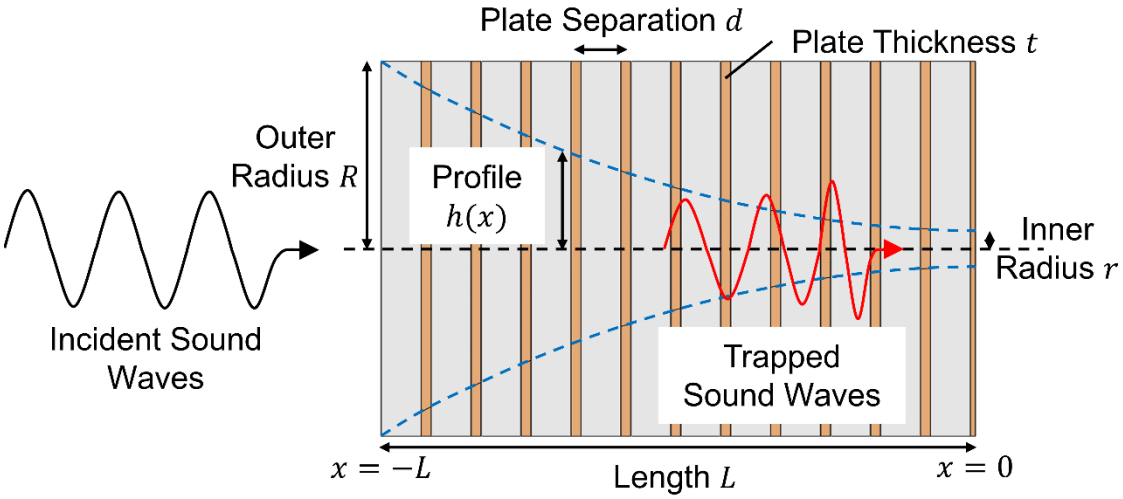

Figure 3: Important design consideration for the SBH.

Table 1: Values of SBH parameters used in this work.

Parameter	Value
Outer radius R (mm)	15
Inner radius r (mm)	1.5
Length of duct L (mm)	30
Number of plates N	6, 12
Distance between adjacent plates d (mm)	5, 2.5
Thickness of each plate t (mm)	0.5
SBH Profile $h(x)$	$h(x) = 15 + \frac{20}{3}x^2$

3. Materials and Methods

3.1. Manufacturing of Samples

The main design of the SSLA consists of $6 \times 6 \times 6$ repetitions of the individual truss lattices with dimensions indicated in Figure 2, with 6 or 12 parallel plates with an SBH cavity profile. For the measurements of sound absorption coefficients, cylindrical samples of diameter 30 mm were manufactured using vat photopolymerization, which is an additive manufacturing technique based on the layer-by-layer photopolymerization of photocurable resins using an ultraviolet (UV) projector. The 3D printer in use in this work is Asiga Max X 27 from Asiga, Australia. The resin used was the standard 405nm UV resin from NOVA3D, chosen due to its high toughness and strength. A layer thickness of 0.1 mm, light intensity of 5 mW/cm^2 and exposure time of 3 s were used during printing. These printing parameters were determined based on the experimental determination of the optimal parameters for the printing of samples using the chosen resin. As-printed parts were cleaned by immersing in isopropyl alcohol for 20 min. The parts were then post-cured in the Asiga Flash UV curing chamber for 30 min. For the mechanical tests, cubic samples, with also repetitions of 6×6×6, were prepared similarly.

3.2. Measurements of Sound Absorption Coefficients

The samples in Section 3.1 were tested using the BWSA SW477 impedance tube to measure the sound absorption coefficient α based on the ISO 10534-2 (1998) standard. The frequency range of interest is from 1000 Hz to 6300 Hz.

3.3. Simulation Methods

A complementary investigation on the sound absorption of the SSLA was done using the pressure acoustics module in COMSOL Multiphysics 5.6. Two types of simulation studies were implemented, one investigates the sound absorption coefficient and energy dissipation mechanism in the SSLA in the frequency domain, and the other investigates the transient behaviour of sound propagation in the SSLA in the time domain to reveal the slow-sound effect. Both studies were done on the SSLA made from the SC-Truss and FCC-Truss due to vastly differing natures of sound absorption. The geometry used for the simulation studies replicates the physical setup in the impedance tube described in Section 2.3, as shown in Figure 4 (a). Such an approach allows direct comparisons between the experimental and simulation results to be made as the sound absorption coefficients of the SSLA were measured experimentally using an actual impedance tube.

The geometry for the first study is shown in Figure 4 (b). To simplify the studies, only the air phase of the experimental setup was modelled, with the boundaries of the tube and SSLA samples, including the thin plates, replaced with hard sound boundary conditions. For computational efficiency, only a quarter of the model was modelled with symmetric boundary conditions. The impedance tube section is modelled as a cylinder of length 235 mm and a diameter of 30 mm. The two microphones were represented as points in the tube, positioned at

a distance of 30 mm and 45 mm from the sample respectively. The fluid medium used in the simulation is air. The properties of the air in the impedance tube follow the default setup in COMSOL. A plane wave of constant pressure amplitude was set to propagate starting from the surface at the end of the impedance tube. The energy losses in the truss-plate hybrid lattice were modelled using the narrow region acoustics module in COMSOL, of which the narrow regions in the sample were assumed to be circular ducts with radii adjusted according to experimental results (Refer to Supplementary Text 1 in the Supplementary Information). The narrow region acoustics model was chosen as it is capable of providing sufficient insights into the energy losses in the system without having to solve for more time- or resource-intensive physical models such as the thermoviscous model. Free tetrahedral mesh of maximum size of 1/6 of the wavelength of sound at 4000 Hz is used for more precise modelling of the acoustic pressure distributions in the domains. The pressure acoustics problem is solved in the frequency domain at frequencies between 1000 Hz and 6300 Hz inclusive, with intervals of 50 Hz.

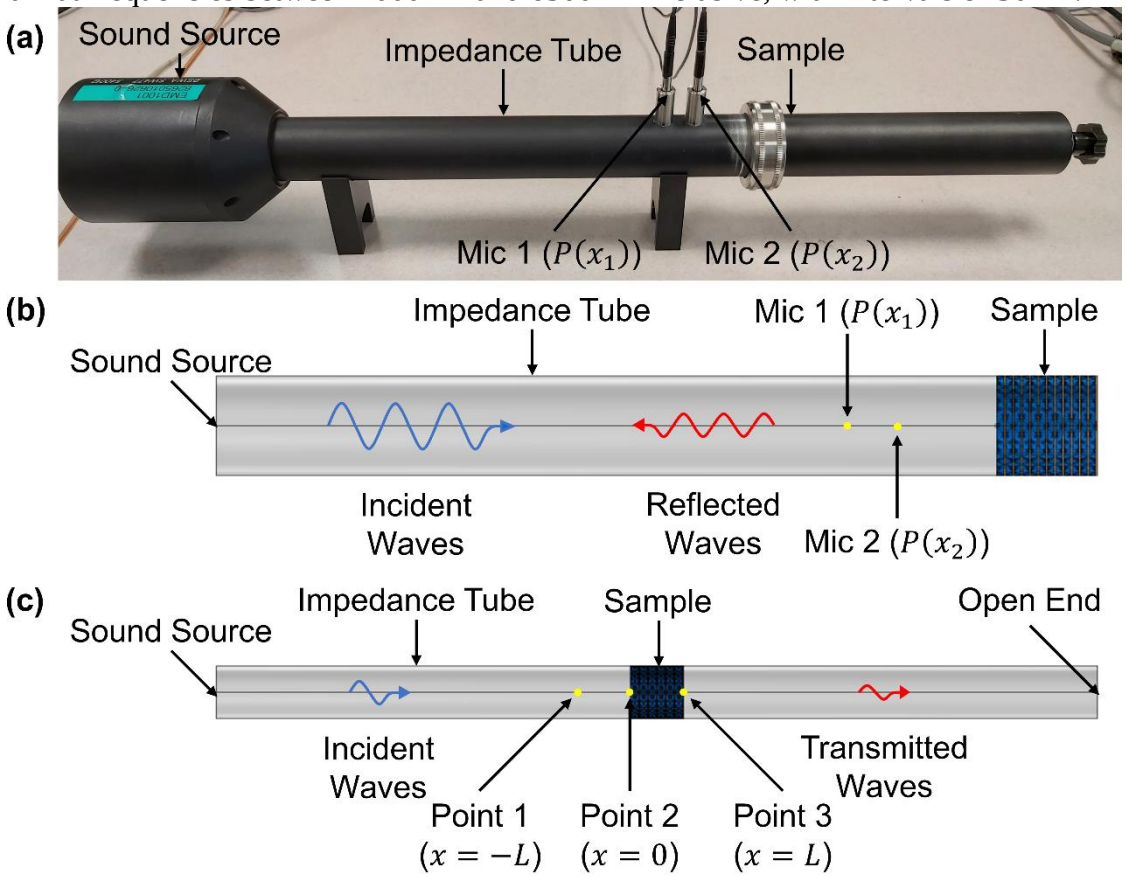

Figure 4: COMSOL geometry used for the simulation studies. (a) Physical setup of the BWSA SW477 impedance tube for sound absorption studies. (b) The COMSOL geometry for the first study mimics the impedance tube setup in Figure 4 (a). (c) COMSOL geometry for the second study.

The sound absorption coefficient for the sample at a particular frequency can be calculated based on the ASTM E1050-19 standards [46]. At any point in the tube, the total sound pressure can be expressed as:

$$P(x) = Ae^{-ikx} + Be^{ikx} \tag{9}$$

where A and B refer to constants, k is the wavenumber as defined in Section 2.2 and the exponent refers to the incoming sound and reflected sound pressures respectively. The sound pressure at microphones 1 and 2 are then expressed as:

$$P(x_1) = Ae^{-ikx_1} + Be^{ikx_1} \tag{10}$$

$$P(x_2) = Ae^{-ikx_2} + Be^{ikx_2} \quad (11)$$

where x_1 and x_2 are the respective distances of each microphone from the sound source. $P(x_1)$ and $P(x_2)$ are then calculated based on integration at the point in COMSOL. The transfer function between points 1 and 2, H_{12}, is then calculated as:

$$H_{12} = \frac{P(x_2)}{P(x_1)} = \frac{e^{-ikx_2} + Re^{ikx_2}}{e^{-ikx_1} + Re^{ikx_1}} \quad (12)$$

where $R = \frac{B}{A}$ is the reflection coefficient. R can then be solved with the current expression and variables. Finally, the absorption coefficient is then calculated as:

$$\alpha = 1 - |R|^2 \quad (13)$$

The entire absorption curve is then calculated over the range of frequencies between 1000 Hz and 6300 Hz. The plane-wave total dissipated power density along a planar section along the diameter of the cylindrical geometry is evaluated at a frequency of 4000 Hz.

The geometry for the transient study is shown in Figure 4 (c). It is almost identical to that of the first study, except that another tube section was attached after the truss-plate hybrid lattice to create a non-reflecting condition. This allows us to study the travelling of wave packets through different checkpoints without being affected by the reflected waves. A Gaussian-like pulse excitation with the centre frequency f_0 was set to propagate from the entrance of the impedance tube, defined as

$$p(t) = -e^{-\left(3f_0(t-T_0)\right)^2} \sin(2\pi f_0 t) \quad (14)$$

where $f_0 = 4000\ Hz$ and $T_0 = \frac{1}{f_0} = 0.25\ ms$. The transient pressure acoustics problem was then solved in the time domain. The sound pressures at three points were extracted and plotted in the time domain at three observation points as labelled in Figure 4 (c): point 1 at a distance of L in front of the sample ($x = -L$); point 2 at the entrance of the truss-plate hybrid lattice ($x = 0$); and point 3 at the end of the sample ($x = L$). The distance between points 2 and 3 is equal to that between points 1 and 2, such that the time delay in the travelling wave packets can infer the reduction of sound speed in the sample.

3.4. Mechanical tests and characterization

Quasi-static compression tests were performed using the Shimadzu AG25-TB universal testing machine at a strain rate of 0.002 s^{-1}. The parallel set of faces normal to the building direction was orientated for compression (Refer to Supplementary Text 2 in the Supplementary Information). The opposing compression faces of the samples were greased to reduce friction during compression. A digital camera was used for the capture of deformation modes. The mechanical properties of concern include the maximum compressive stress, plateau end stress and strain, energy absorption and absorption efficiency, as well as the specific energy absorption (SEA). In this paper, the SEA is calculated based on the work done during the compression as [38, 39]:

$$SEA = \frac{\int_0^{\varepsilon_d} \sigma \cdot d\varepsilon}{\rho_c} \quad (15)$$

where σ and ε are the compressive stress and strain respectively, ε_d is the densification strain and ρ_c the density of the lattices. The densification strain is obtained from the stress-strain plots by identifying the points on the curves at which the lattices have fully densified.

4. Results and Discussions

4.1. Manufacturing of Samples

Digital photographs of the printed samples for the measurements of sound absorption coefficients are shown in Figure 5. A subset of the printed lattices was sectioned to reveal the lattice struts, plates and SBH cavity. It can be seen that the samples are of high print quality

that highly resembles the computer-aided design, with minimal printing defects. It was noted that no support materials were added between struts or plates during printing. This observation shows that the SSLA can be manufactured easily using AM processes such as vat photopolymerization, with high dimensional tolerances and minimal printing defects.

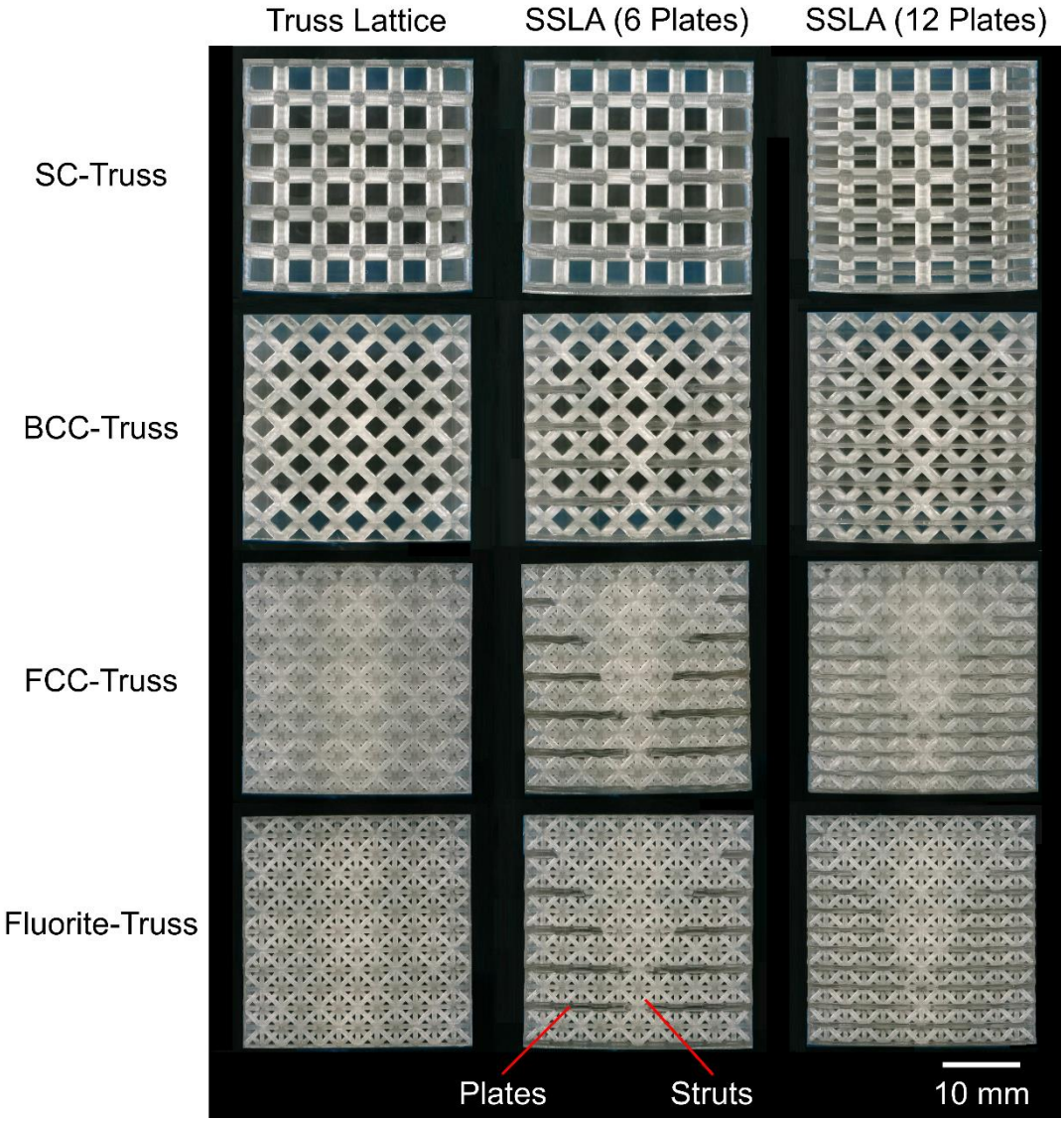

Figure 5: Printed truss-plate hybrid samples from the vat photopolymerization process (a) SC-Truss, (b) BCC-Truss, (c) FCC-Truss, (d) Fluorite-Truss.

4.2. Sound Absorption Coefficients

The sound absorption coefficients for all the samples obtained experimentally are plotted in Figure 6. The means and standard deviations of the sound absorption coefficients for various frequency bands are plotted in Figure 7. Based on both figures, the sound absorption performances of the pure truss lattices are notably poor, with the mean sound absorption coefficients below 0.5. Each of these truss lattices contains one sound absorption peak within a frequency band of 2000 to 3000 Hz, which indicates a form of resonant behaviour exhibited by the lattices. The results obtained are similar to those reported in several studies in the literature [23, 40, 41].

The sound absorption of the truss-SBH hybrid lattices is significantly higher than that of the truss lattices alone as shown in Figure 7. The average sound absorption coefficients in most frequency bands are more than doubled by simply adding 6 plates into the lattice. This suggests

that the addition of the SBH-like plates in the design of the truss lattices can increase the sound absorption performances of the hybrid lattices. Also, we observe an increasing number of absorption peaks, reminiscent of the sound absorption studies on sonic black holes in the scientific literature, hence suggesting the inclusion of the sound absorption performance of the SBH into that of the proposed lattices. The actual sound absorption mechanisms for the hybrid lattices will be discussed in the next section. The increase in the number of absorption peaks also increased the standard deviation of the absorption coefficients for all the lattices. This indicates a large variability in sound absorption coefficients especially close to the absorption peaks, where the difference between the highest and lowest points can be up to 0.6. For most lattices, the inclusion of more SBH plates tends to provide an increase in mean sound absorption coefficients by about 7% throughout the frequency bands of interest. This corroborates with the scientific literature that increasing the number of rings in the SBH tends to improve the sound absorption performance of the SBH duct. The standard deviation of the absorption coefficients showed a slight increase from the 6-plate SSLAs due to the larger number of absorption peaks within the whole frequency range. However, the standard deviation of the sound absorption coefficients decreased at the frequency band of 4000 – 6300 Hz while keeping the coefficients consistently high, which indicates the high potential of these truss-SBH lattices to be used as broadband sound absorbers. The sound absorption performance of SSLA based on the SC-Truss differs significantly from the other lattices, and the reasons for such a variation will be investigated in the subsequent subsection.

Another interesting observation is that truss only lattices exhibit one main peak for sound absorption, centred at around 2800 Hz for both SC and FCC cases. By embedding SBH plates, the occurrence of the first peak is shifted much earlier to 1600 Hz for the SC case, and even below 1000 Hz for the FCC case. This means that the SBH inclusion not only increases the damping magnitude through its energy focusing mechanism but also enhances the sub-wavelength performance through its slowing-wave property. More information on the effects of the SBH cavities on the frequency peaks is found in Supplementary Text 3 in the Supplementary Information. It is worth noting that the acoustic wavelength at 1000-1600 Hz is around 0.2-0.34 m, which is more than 10 times the physical thickness of the lattice sample. Thus, the proposed SSLA provide a new way of constructing a sub-wavelength sound absorber. The detailed mechanisms will be discussed in the next section with the help of energy dissipation and transient simulations. Also note that the lengths of the SSLAs in this study are kept constant at 30 mm and it is well established that changing the lengths of an acoustic absorber has effects on its sound absorption performances. The effects of changing the length of the SSLAs while keeping constant other parameters such as the outer and inner radii, as well as the distance between adjacent plates are discussed in Supplementary Text 4 in the Supplementary Information.

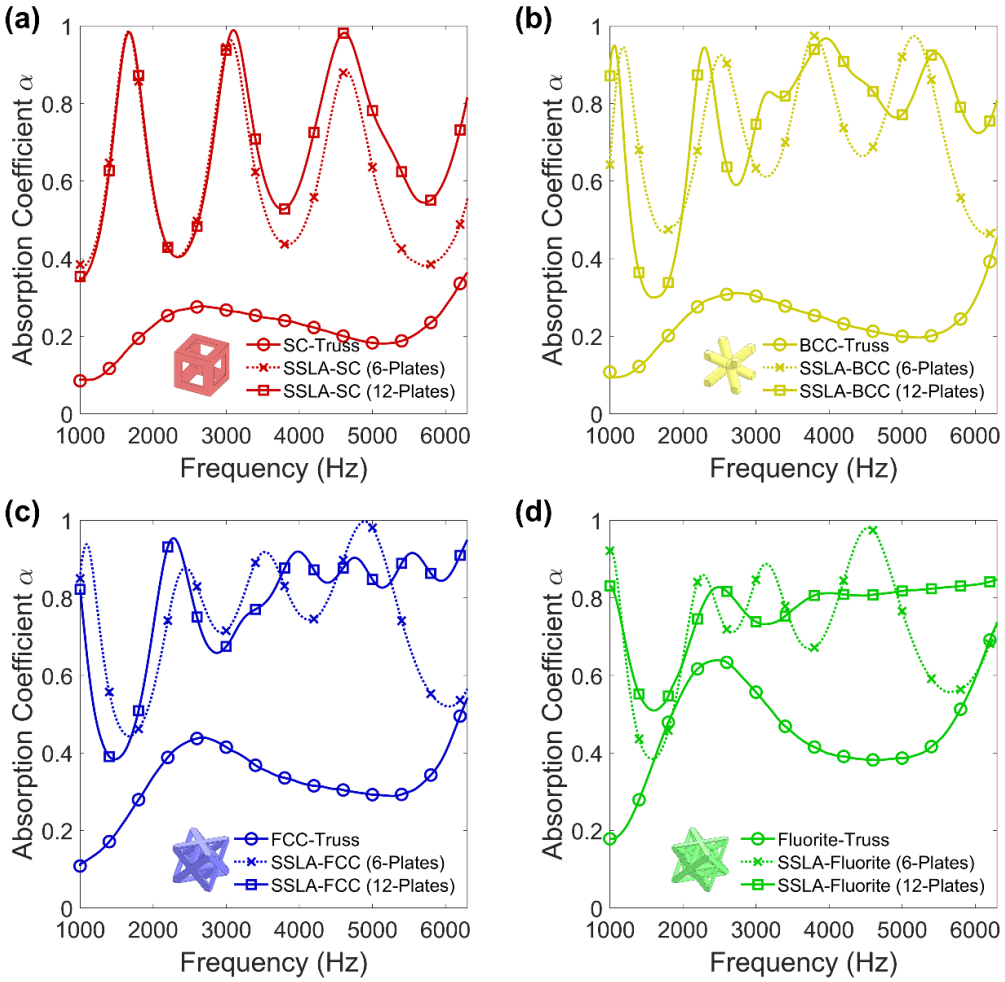

Figure 6: Plots of sound absorption coefficients for (a) SC-Truss, (b) BCC-Truss, (c) FCC-Truss and (d) Fluorite-Truss. Each subfigure contains sound absorption coefficients for three cases, mainly truss lattice only, truss lattice with 6 SBH plates and truss lattice with 12 SBH plates.

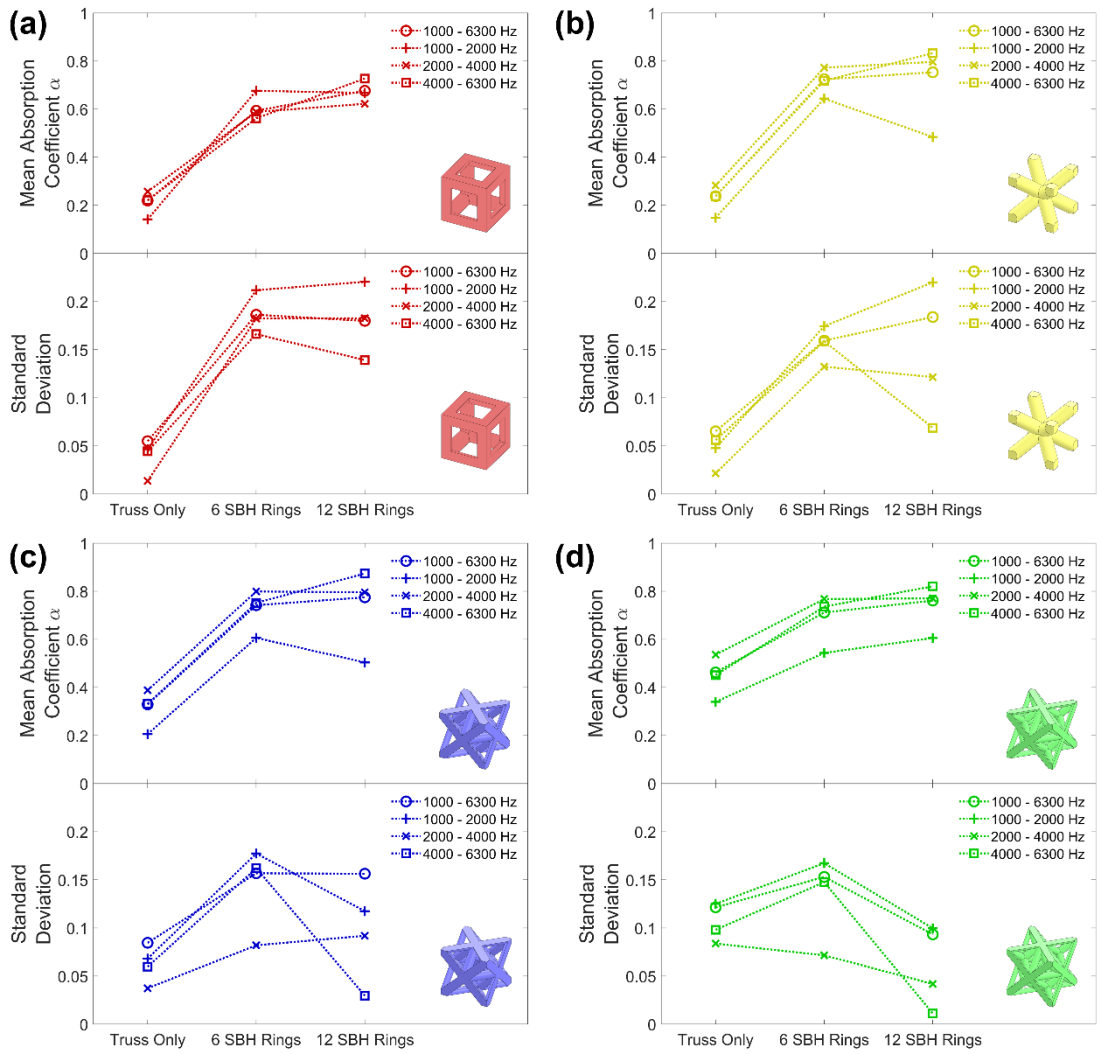

Figure 7: Plots of means and standard deviations of the sound absorption coefficients for (a) SC-Truss, (b) BCC-Truss, (c) FCC-Truss and (d) Fluorite-Truss. Values were calculated based on data at a frequency band of 1000 to 6300 Hz and three sub-bands. Each subfigure contains sound absorption coefficients for three cases, mainly truss lattice only, truss lattice with 6 SBH plates and truss lattice with 12 SBH plates.

As a form of validation of the simulation results as detained in Section 2.4, the sound absorption coefficients obtained from both experiments and simulation results were plotted as shown in Figure 8. Apart from the geometric profile of the SBH, the damping loss in the lattice structures also plays an important role in determining the magnitude of sound absorption. Here, the air phase in the lattice structures is simply treated as a narrow region acoustic domain, [42]. The narrow region parameters used in the simulations are tabulated in Supplementary Text 1 in the Supplementary Information. The closeness in the sound absorption distributions between the experimental and simulation results was observed, particularly the relative magnitudes of sound absorption coefficients and the number and relative positions of the absorption peaks. Therefore, this suggests that the narrow region acoustics module is generally sufficient to model the sound absorption behaviour of the SSLA. That being said, it is important to note that the narrow region parameters used in the simulations were fitted from experimental measurements. As such, the numerical models used in this study need to be tweaked to SSLAs with slight changes to their geometries such as the number of plates or the strut diameters, by

obtaining the narrow region acoustics parameter by performing regression of the numerical model onto actual experimental data.

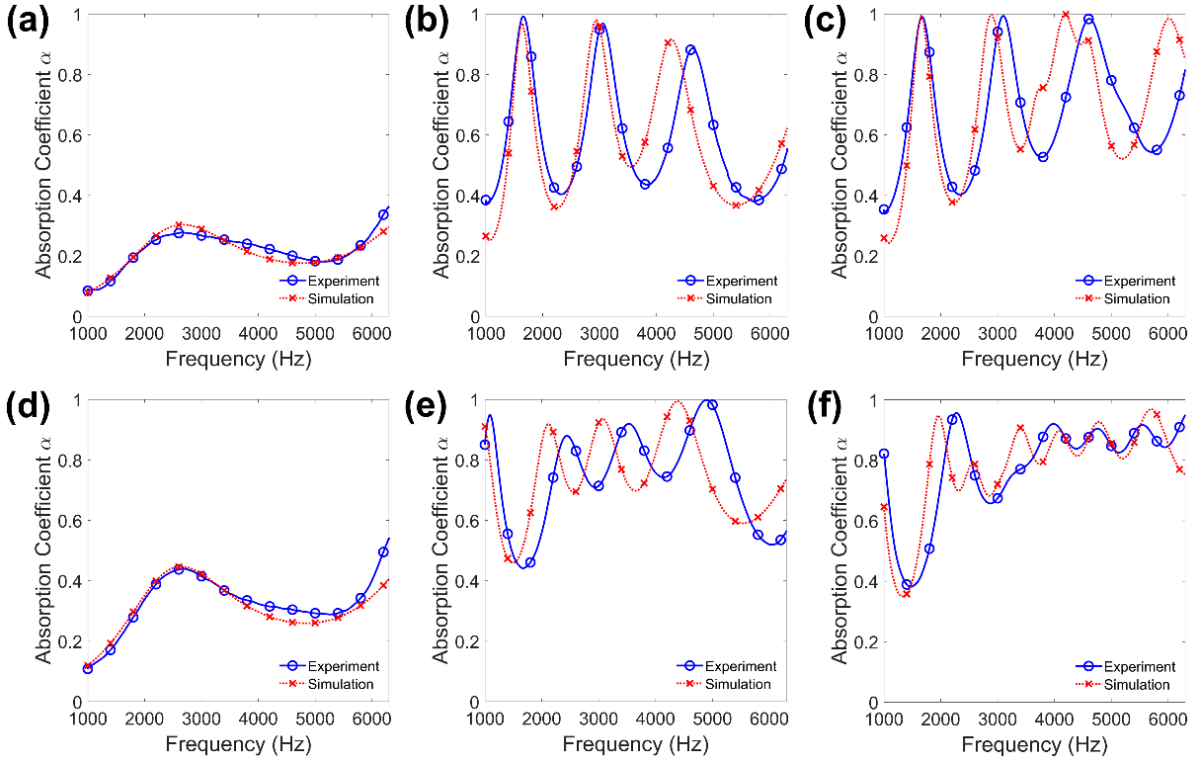

Figure 8: Plots of sound absorption coefficients obtained from experiments and simulations for (a) SC-Truss, (b) SC-Truss with 6 SBH plates, (c) SC-Truss with 12 SBH plates, (d) FCC-Truss, (e) FCC-Truss with 6 SBH plates, and (f) FCC-Truss with 12 SBH plates.

4.3. Sound Absorption Mechanisms

The hybrid lattice structures proposed in this work exploit the unique slow-sound and energy-focusing properties of SBH to enhance the sound absorption of conventional porous structures. The simulation model validated in the previous section is used to reveal the detailed mechanisms for enhanced sound absorption. To investigate the sound energy losses within the SSLA, the heat maps of the plane wave sound dissipation densities over the cross-section of the samples were plotted. Furthermore, to trace the variation of sound speed within the hybrid lattices, the total acoustic pressures at the three points were tracked with time and plotted on the same axes.

4.3.1. Sound absorption of SC-Truss lattices with and without SBH plates

The energy dissipation map from the frequency domain simulation and the pressure signals from the transient simulation for the SC-Truss are shown in Figures 9 (b) and (c), respectively. From the dissipation heat map, it can be seen that the sound energy from the plane wave was dissipated on a layer-by-layer basis, with the most dissipation from the first layer and decreasing dissipation as the sound wave propagates through the successive layers. As noted in previous studies on sound absorption of truss lattices [22, 23], the main mechanism of sound absorption is based on resonance akin to micro-perforated panels. This can also be seen from the significantly higher energy losses at the necks of each SC lattice cell. The transient pressure plot indicates that the reduction in sound speed in the SC-Truss is minimal, where the time gaps for the acoustic pressures to reach a local maximum between two adjacent points are similar.

When six plates are added to the lattice design, Figure 9 (d) shows the corresponding energy loss heat map. The energy loss distribution differs significantly from Figure 9 (b) in that most of the energy losses are confined in the inner cavity marked out by the holes of the plates. Furthermore, most of the energy losses are concentrated at the rims of the holes and the narrow necks of the SC-Truss cells, with significantly higher energy loss densities than in the previous case. Therefore, it can be inferred that the sound energy dissipation by resonance effects is still present in the SSLA, but is concentrated at the tip of the SBH plates. Figure 9 (e) shows the transient acoustic pressures in the SC-Truss with 6 SBH plates. While the pressure distributions at Points 1 and 2 are similar to Figure 9 (c) in the first half millisecond, the acoustic pressure distribution at Point 3 shows a large variation from Figure 9 (c), as outlined below.

(1) It is noted that the amplitude of acoustic pressures at Point 3 is much lower in the truss-plate hybrid lattice than in the SC-Truss owing to a stronger sound reduction effect. We note from Figure 9 (d) that most of the energy dissipation occurs at the first half of the truss-plate hybrid lattice with relatively high loss densities. Therefore, the sound energy at the termination would be much lower.

(2) The time gap between the first local maxima for Points 2 and 3 is significantly greater than the time gap between that Points 1 and 2. It can be noted that the time gaps indicate the time taken for sound to travel a distance L, it can then be inferred that the speed of sound between Points 2 and 3 (i.e. within the truss-plate lattice) is significantly lowered by about 70% (refer to Supplementary Text 5 in the Supplementary Information). Therefore, the proposed truss-plate hybrid lattice is successful in decelerating an incoming sound wave. As the absorption frequency has a proportional relationship with the sound speed, a reduction in the sound speed will move the effective frequencies toward lower frequencies. This explains the early occurrence of the absorption peaks as observed in Figure 6 (a)—(c), where the first peak is shifted from 2800 Hz to 1600 Hz by embedding SBH into the truss lattice.

(3) The period of the acoustic pressure at Point 3 is significantly higher than that at the other two points. Measurements based on two consecutive maxima indicate that the period of the acoustic pressure at Point 3 is about 0.738 ms, which is about 4 times higher than the period of the acoustic pressure at Points 1 and 2. This again implies that sound speed in the truss-plate hybrid lattice is significantly decreased.

(4) Through the deceleration effect, any incoming acoustic wave will be trapped in the lattice for a longer time, allowing any energy damping effects within the lattice to act on the sound waves for a longer time, hence resulting in higher energy reductions.

Figures 9 (f) and (g) show the energy loss density heat map and transient pressure plot when 12 SBH plates were added to the SC-Truss. Similar observations can be made from the case with 6 SBH plates, such as the energy dissipation being focused within the inner cavity and the reduction in sound speed and frequency. However, it can be seen that the energy focusing effects of the SBH plates are stronger and the energy dissipation densities are higher when more SBH plates were added. However, the addition of SBH plates at locations in between the necks of the SC-Truss poses few additional effects on the sound absorption mechanism of the truss-plate hybrid lattice. This explains the similarity in absorption coefficients for the SC-Truss with 6 or 12 ABH plates as seen in Figure 6 (a). Note that perfect absorption occurs when the losses compensate the leakage of the system.

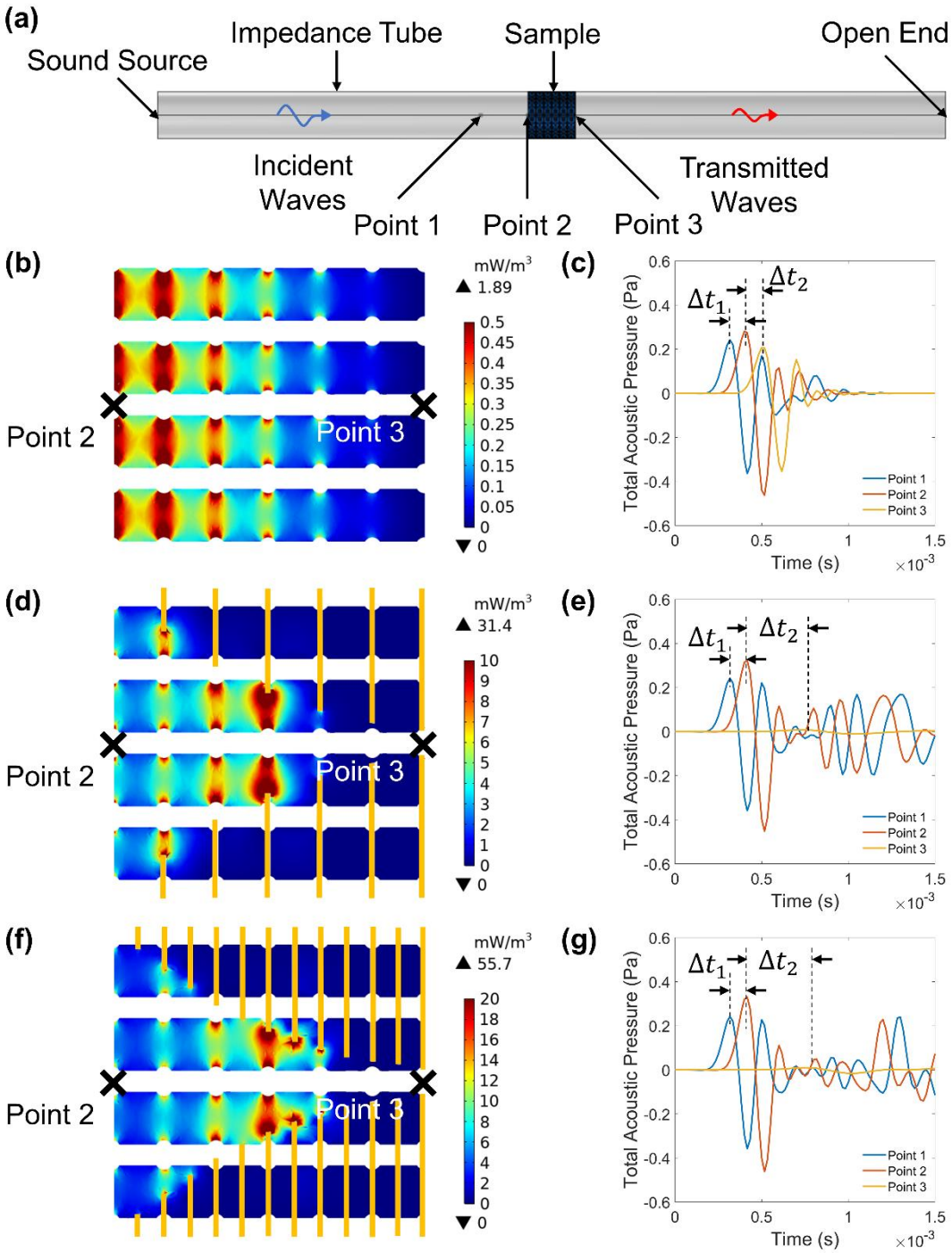

Figure 9: (a) COMSOL geometry for the transient study, reproduced from Figure 4 (c). (b) A plot of plane-wave total dissipated power density for SC-Truss at a frequency of 4000 Hz. (c) Plots of total acoustic pressure obtained from transient simulation study for SC-Truss. (d) A plot of plane-wave total dissipated power density for SC-Truss with 6 SBH plates at a frequency of 4000 Hz. Orange lines indicate the SBH plates within the lattice. (e) Plots of total acoustic pressure obtained from transient simulation study for SC-Truss with 6 SBH plates. (f) A plot of plane-wave total dissipated power density for SC-Truss with 12 SBH plates at a frequency of 4000 Hz. Orange lines indicate the SBH plates within the lattice. (g) Plots of total acoustic pressure obtained from transient simulation study for SC-Truss with 12 SBH plates.

4.3.2. Sound absorption of FCC-Truss lattices with and without SBH plates

The analysis of the plane-wave total dissipated power density and transient acoustic pressures were repeated for the FCC-Truss, as shown in Figure 10. The labelling for each subfigure in Figure 9 and Figure 10 is similar.

While the absorption curves between the SC-Truss and FCC-Truss may differ significantly, it can be seen that most of the effects discussed for the SC-Truss also apply to the FCC-Truss, with differences mainly in the geometry of the truss lattices. As seen in the power dissipation heat maps in Figure 10, the energy dissipation from resonating cells also applies to the FCC-Truss as seen from the higher energy loss densities near the struts of the truss lattices. Similar to the case of the SC-Truss, the FCC-Truss dissipates energy layer-by-layer, and the addition of SBH plates focuses most of the energy dissipation within the inner SBH cavities. However, the addition of plates has an improved energy loss effect as compared to the SC-Truss. This is likely due to the location of the additional plates coinciding with the location of some of the strut intersections in the FCC-Truss lattice, which are also locations of significant sound energy dissipations by resonance.

The plots of transient acoustic pressures in Figure 10 are similar to that in Figure 9. However, the amplitudes of acoustic pressures at Point 3 are notably higher than in Figure 9. This suggests that the sound absorption of the initial transient sound wave is lesser than in the SC-Truss cases. An explanation for this increase is due to the smaller strut diameters of the FCC-Truss as compared to the SC-Truss, which implies that the necks of each resonant cell in the FCC-truss are wider, which weakens the energy dissipation by resonance effects.

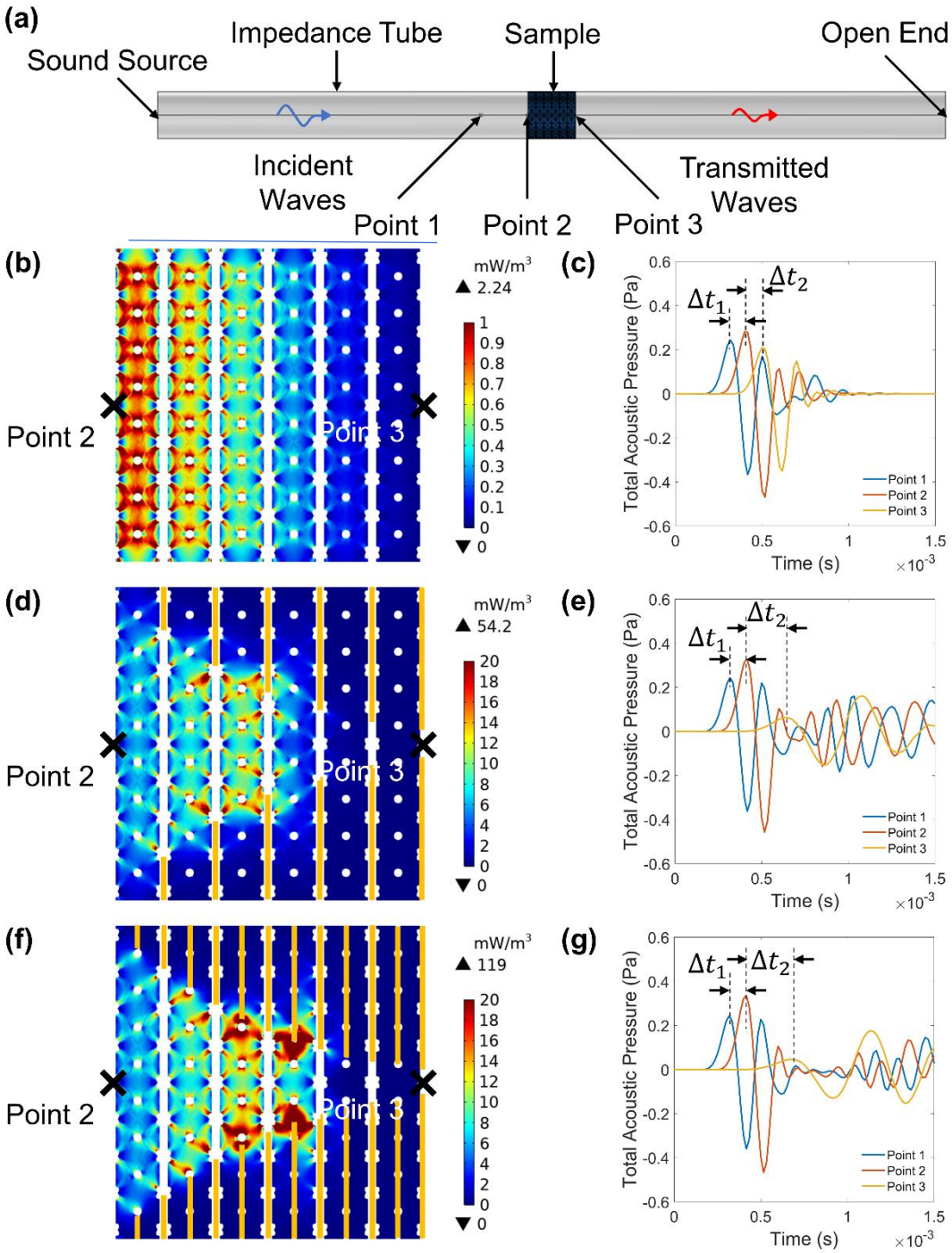

Figure 9: (a) COMSOL geometry for the transient study, reproduced from Figure 4 (c). (b) A plot of plane-wave total dissipated power density for FCC-Truss at a frequency of 4000 Hz. (c) Plots of total acoustic pressure obtained from transient simulation study for FCC-Truss. (d) A plot of plane-wave total dissipated power density for FCC-Truss with 6 SBH plates at a frequency of 4000 Hz. Orange lines indicate the SBH plates within the lattice. (e) Plots of total acoustic pressure obtained from transient simulation study for FCC-Truss with 6 SBH plates. (f) A plot of plane-wave total dissipated power density for FCC-Truss with 12 SBH plates at a frequency of 4000 Hz. Orange lines indicate the SBH plates within the lattice. (g) Plots of total acoustic pressure obtained from transient simulation study for FCC-Truss with 12 SBH plates.

4.4. Mechanical Properties

Figure 11 shows the compressive stress-strain curves of the truss-plate lattice samples as compared to the base truss lattice constituent. The calculated mechanical properties were collated in Supplementary Text 6 in the Supplementary Information. The deformation behaviours of the lattices are collated in Figure 12. We observed that the distributions of the FCC-Truss and Fluorite-Truss lattices are similar, while the distributions of the SC-Truss and BCC-Truss vary significantly. For both the SC-Truss and BCC-Truss, the addition of SBH plates increases the compressive stress values for most strain values. The stress plateau region tends to be reduced as more SBH plates were added, implying the addition of the plate architecture lowers the densification strain of the hybrid lattices. Moreover, for the BCC-Truss, the stress plateau becomes more even as SBH plates were added. For both the FCC-Truss and Fluorite-Truss lattices, the addition of SBH plates increases the slope of the stress plateau region and decreases the densification strain from about 0.6 to about 0.4.

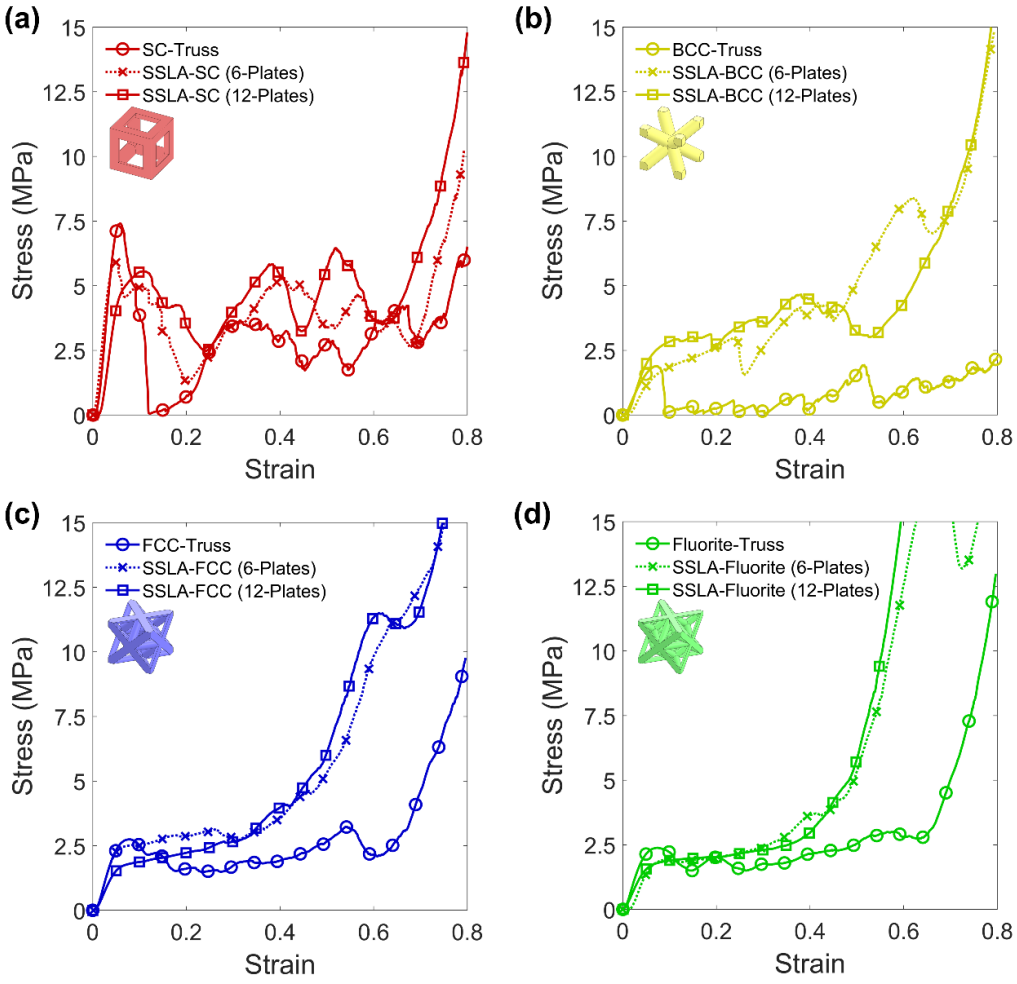

Figure 11: Plots of stress-strain distributions for (a) SC-Truss, (b) BCC-Truss, (c) FCC-Truss and (d) Fluorite-Truss. Each subfigure contains stress-strain curves for three cases, mainly truss lattice only, truss lattice with 6 SBH plates and truss lattice with 12 SBH plates.

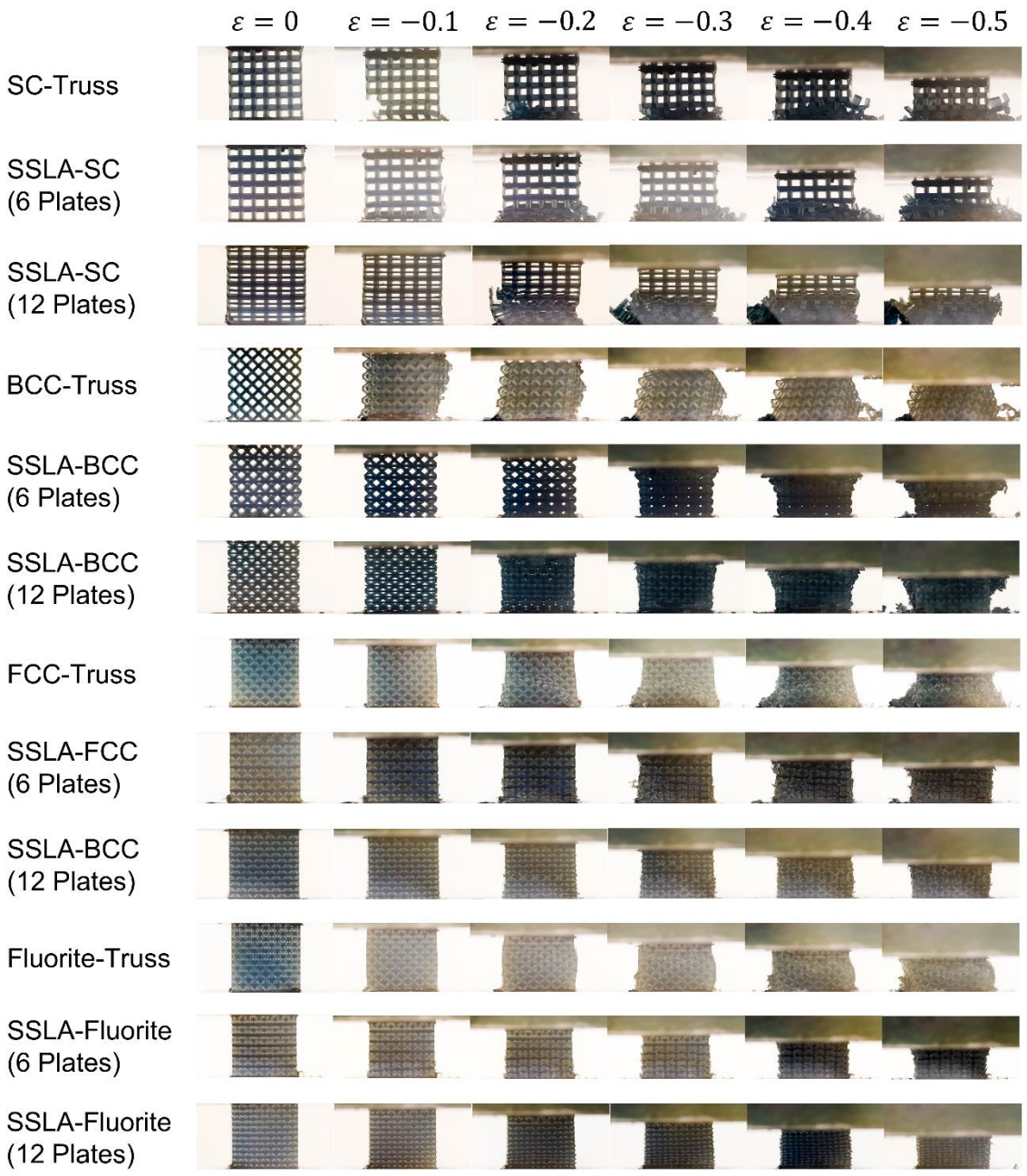

Figure 12: Experimentally obtained deformation behaviour of the pure truss lattices, truss lattices with 6 SBH plates and truss lattices with 12 SBH plates.

The scatter plots of the energy absorption efficiency and SEA of the truss-plate lattices against relative density are shown in Figure 13. Note that the addition of SBH plates into the truss lattice architecture does not affect the dimensions of the truss lattice struts, hence increasing the relative density of the samples. It can be seen that the addition of SBH plates into the truss lattice architecture is associated with an increase in the absorption efficiency, especially for the SC-Truss and BCC-Truss lattices. This is attributed to the addition of the plates at the location of stress concentration of the original truss lattices. As observed in the deformation sequences in Figure 13, the plates reduce the occurrence of sudden fractures and collapses of lattice struts that can produce the valley-like stress plateau region in stretch-dominate cellular structures. This causes the plateau region to become more uniform, which increases the absorption efficiency. From Figure 14 (b), the addition of SBH plates is associated with an increase in SEA for SC-Truss and BCC-Truss lattice structures, which can be attributed to the increase in

compressive stresses in the plateau region and the more uniform plateau region, while minimising the decrease in densification strain. However, there is a decrease in SEA for FCC-Truss and Fluorite-Truss lattice structures as the SBH plates were added, mostly attributed to the significantly brought forward strains with minimal increase in compressive strength.

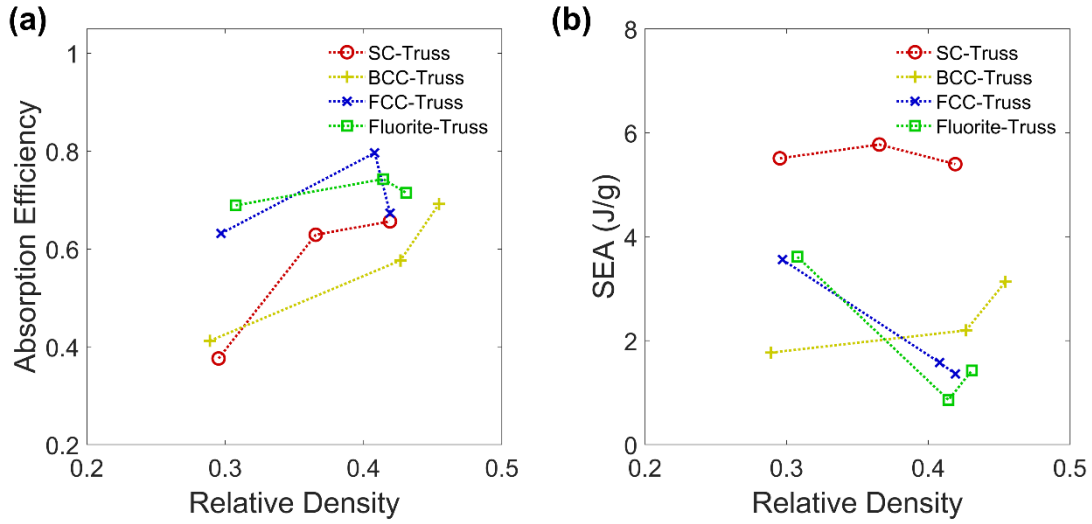

Figure 13: Scatter plots of (a) energy absorption efficiency and (b) SEA against relative density.

5. Further Discussions

In this work, we presented a novel lattice design concept based on the integration of conventional strut lattice design with the principles of the SBH. Sound absorption measurements conducted on these lattices indicated a vast improvement in sound absorption performances from a mean absorption coefficient of 0.31 for the pure truss lattices to an average absorption coefficient of 0.72 for the truss-ABH lattices. Compression tests indicate that the compressive strength of these lattices was generally increased. The addition of ABH plates to SC-Truss and BCC-Truss lattices also provided an increase in energy absorption, absorption efficiency and SEA as seen in Figure 13. Therefore, these novel SSLAs are advantageous with both the excellent sound absorption properties of the SBH and the mechanical robustness of lattices; as such presenting unprecedented properties not found in either constituent or traditional materials such as foams, pure truss lattices and perforated panels [10, 22, 42, 43]. Such multifunctional materials hence find high practical values and high commercial values as practical acoustic materials. Specific to the SSLAs, one can think of them as materials that can function as both a lattice structure and a sound absorber, hence finding important applications as lightweight acoustic and mechanical energy and impact absorbers.

Furthermore, through the transient simulation studies, we have identified the locations of the acoustic energy losses within our truss-SBH structures and their relative magnitudes of losses. Such studies are valuable in advancing the scientific understanding of the sound absorption mechanisms of not only our SSLA but also within SBHs and truss lattices in general. It is noted that many studies acknowledged that sound absorption within lattice structures comes in the form of viscous and thermal losses [41, 44, 45], structural damping [42, 46], as well as resonance effects [22]. However, most studies may face significant challenges in identifying the major locations where most of the acoustic energy may be dissipated based on numerical models alone, which may lead to a risk of haphazard design optimization or non-optimal sound absorbers. Through this study, by emphasising the locations of significant energy losses within the absorbers obtained through finite element analysis, the optimization of the sound absorbers

for various applications can be done through a more targeted approach, resulting in significant time and cost savings.

Lastly, SBH concepts are generally limited to physical theory or laboratory research due to their difficulty to be manufactured in large quantities. In our case, there are significant difficulties in manufacturing a pure duct SBH oriented from bottom to top without support material, and one may find it difficult to remove the support materials when added. However, the inclusion of the truss lattices allows the above difficulty to be circumvented due to the self-supporting nature of the lattices. Further experimental investigations show that the SSLA exhibits comparable sound absorption performances as compared to the pure SBH, as shown in Supplementary Text 7 in the Supplementary Information. Hence, this approach shows high potential in the manufacturing of SBHs in large quantities. This makes it possible to make significant progress in the creation of lightweight noise control structures with superior noise reduction performances, further aiding in the resolution of urban noise pollution.

6. Conclusions

In this work, we presented a novel class of slow-sound lattice absorbers (SSLA) by including a set of plates resembling an SBH profile into the design of truss lattices based on the mimic of Bravais lattice structures. The truss lattices considered were based on the SC, BCC, FCC and fluorite crystal structures. The truss-plate lattices were printed using vat photopolymerization with the addition of either 6 or 12 SBH plates. Measurements of the sound absorption coefficients of the printed samples indicated that the sound absorption coefficients of the SSLA are more than double that of the pure strut lattices, with the addition of more SBH plates increasing the overall absorption coefficients. Simulations conducted based on the lattices revealed that the SSLA has successfully incorporated the sound speed reduction effects of the SBH alongside the sound absorption mechanism of resonating cells inherent in truss lattice structures. The SBH plates have the effects of focusing most of the sound power dissipation within the SBH cavity while decreasing the sound speed and frequency of the sound waves. By positioning the SBH plates to coincide with the locations of the necks of the resonant cells in the truss lattices, the energy dissipation density at the resonant cells can be amplified. This work marks significant progress in the design of lattices as sound absorbers based on novel sound absorption physics, in particular, the incorporation of sound speed reduction mechanisms to amplify the sound wave dissipations within lattices. This work marks significant progress in the design of lattices as sound absorbers based on novel sound absorption physics, in particular, the incorporation of sound speed reduction mechanisms to amplify the sound wave dissipations within lattices. The SSLA, with its excellent mechanical and sound absorption properties, find high practical and commercial values as practical acoustic material. Furthermore, the SSLA design circumvents the manufacturing limitations of pure SBHs, allowing them to be manufactured in large quantities. This work also serves to provide a guide for materials researchers on the inclusion of such novel physics in the design of better lattice sound absorbers for practical applications.

Author contribution statement

Jun Wei Chua: Conceptualization, Methodology, Validation, Investigation, Writing - Original Draft and Editing. **Xinwei Li**: Conceptualization, Methodology, Resources, Writing - Original Draft, Review and Editing. **Xiang Yu**: Conceptualization, Methodology, Validation, Resources, Supervision, Writing - Review & Editing. **Wei Zhai**: Conceptualization, Validation, Resources, Funding acquisition, Supervision, Writing - Review & Editing.

Declaration of competing interest

The authors declare that they have no known competing financial interests or personal relationships that could have appeared to influence the work reported in this paper. Any opinions, findings and conclusions or recommendations expressed in this material are those of the author(s) and do not reflect the views of NUS or A*STAR.

Acknowledgements

This research is supported by A*STAR under its AME YIRG Grant (Project No. A20E6c0099).

References

[1] Kumar S, Lee H. The Present and Future Role of Acoustic Metamaterials for Architectural and Urban Noise Mitigations. Acoustics. 2019;1:590-607.

[2] Jia C, Li L, Liu Y, Fang B, Ding H, Song J, et al. Highly compressible and anisotropic lamellar ceramic sponges with superior thermal insulation and acoustic absorption performances. Nature communications. 2020;11:1-13.

[3] Johnston W, Sharma B. Additive manufacturing of fibrous sound absorbers. Additive Manufacturing. 2021;41.

[4] Gai X-L, Xing T, Li X-H, Zhang B, Wang W-J. Sound absorption of microperforated panel mounted with helmholtz resonators. Applied Acoustics. 2016;114:260-5.

[5] Tang Y, Ren S, Meng H, Xin F, Huang L, Chen T, et al. Hybrid acoustic metamaterial as super absorber for broadband low-frequency sound. Scientific reports. 2017;7:43340.

[6] Khosravani MR, Reinicke T. Experimental characterization of 3D-printed sound absorber. European Journal of Mechanics - A/Solids. 2021;89.

[7] Yang M, Chen S, Fu C, Sheng P. Optimal sound-absorbing structures. Materials Horizons. 2017;4:673-80.

[8] Mi Y, Zhai W, Cheng L, Xi C, Yu X. Wave trapping by acoustic black hole: Simultaneous reduction of sound reflection and transmission. Applied Physics Letters. 2021;118.

[9] Gautier F, Krylov VV. Special issue: Recent advances in Acoustic Black Hole research. Journal of Sound and Vibration. 2020;476.

[10] Zhai W, Yu X, Song X, Ang LYL, Cui F, Lee HP, et al. Microstructure-based experimental and numerical investigations on the sound absorption property of open-cell metallic foams manufactured by a template replication technique. Materials & Design. 2018;137:108-16.

[11] Zhang X, Wang Y, Ding B, Li X. Design, fabrication, and mechanics of 3D micro-/nanolattices. Small. 2020;16:1902842.

[12] Benedetti M, Du Plessis A, Ritchie R, Dallago M, Razavi S, Berto F. Architected cellular materials: A review on their mechanical properties towards fatigue-tolerant design and fabrication. Materials Science and Engineering: R: Reports. 2021;144:100606.

[13] Schaedler TA, Jacobsen AJ, Torrents A, Sorensen AE, Lian J, Greer JR, et al. Ultralight metallic microlattices. Science. 2011;334:962-5.

[14] Zheng X, Lee H, Weisgraber TH, Shusteff M, DeOtte J, Duoss EB, et al. Ultralight, ultrastiff mechanical metamaterials. Science. 2014;344:1373-7.

[15] Zhang X, Vyatskikh A, Gao H, Greer JR, Li X. Lightweight, flaw-tolerant, and ultrastrong nanoarchitected carbon. Proceedings of the National Academy of Sciences. 2019;116:6665-72.

[16] Bauer J, Kraus JA, Crook C, Rimoli JJ, Valdevit L. Tensegrity Metamaterials: Toward Failure-Resistant Engineering Systems through Delocalized Deformation. Advanced Materials. 2021;33:2005647.

[17] Plocher J, Panesar A. Effect of density and unit cell size grading on the stiffness and energy absorption of short fibre-reinforced functionally graded lattice structures. Additive Manufacturing. 2020;33:101171.

[18] Saleh MS, Hu C, Brenneman J, Al Mutairi AM, Panat R. 3D printed three-dimensional metallic microlattices with controlled and tunable mechanical properties. Additive Manufacturing. 2021;39.
[19] Guo X, Ding J, Li X, Qu S, Song X, Fuh JYH, et al. Enhancement in the mechanical behaviour of a Schwarz Primitive periodic minimal surface lattice structure design. International Journal of Mechanical Sciences. 2021:106977.
[20] Jam A, du Plessis A, Lora C, Raghavendra S, Pellizzari M, Benedetti M. Manufacturability of lattice structures fabricated by laser powder bed fusion: A novel biomedical application of the beta Ti-21S alloy. Additive Manufacturing. 2022;50:102556.
[21] Askari M, Hutchins DA, Thomas PJ, Astolfi L, Watson RL, Abdi M, et al. Additive manufacturing of metamaterials: A review. Additive Manufacturing. 2020:101562.
[22] Li X, Yu X, Chua JW, Lee HP, Ding J, Zhai W. Microlattice Metamaterials with Simultaneous Superior Acoustic and Mechanical Energy Absorption. Small. 2021;17:e2100336.
[23] Kassim DH, Putra A, Hamid MFSC, Alkahari MR. Sound Absorption of BCC Lattice Structures. In: Sabino U, Imaduddin F, Prabowo AR, editors.: Springer; 2020. p. 69-79.
[24] Sun X, Jiang F, Wang J. Acoustic Properties of 316L Stainless Steel Lattice Structures Fabricated via Selective Laser Melting. Metals. 2020;10:111.
[25] Deshmukh S, Ronge H, Ramamoorthy S. Design of periodic foam structures for acoustic applications: Concept, parametric study and experimental validation. Materials & Design. 2019;175:107830.
[26] Yang W, An J, Chua CK, Zhou K. Acoustic absorptions of multifunctional polymeric cellular structures based on triply periodic minimal surfaces fabricated by stereolithography. Virtual and Physical Prototyping. 2020;15:242-9.
[27] Cheng L-W, Cheng C-W, Chung K-C, Kam T-Y. Sound absorption of metallic sound absorbers fabricated via the selective laser melting process. Applied Physics A. 2017;123:37.
[28] Zieliński TG, Opiela KC, Pawłowski P, Dauchez N, Boutin T, Kennedy J, et al. Reproducibility of sound-absorbing periodic porous materials using additive manufacturing technologies: Round robin study. Additive Manufacturing. 2020;36:101564.
[29] Monkova K, Vasina M, Monka PP, Kozak D, Vanca J. Effect of the Pore Shape and Size of 3D-Printed Open-Porous ABS Materials on Sound Absorption Performance. Materials (Basel). 2020;13.
[30] Mironov M. Propagation of a flexural wave in a plate whose thickness decreases smoothly to zero in a finite interval. 1988;34:318-9.
[31] Pelat A, Gautier F, Conlon SC, Semperlotti F. The acoustic black hole: A review of theory and applications. Journal of Sound and Vibration. 2020;476.
[32] Li H, Touzé C, Pelat A, Gautier F, Kong X. A vibro-impact acoustic black hole for passive damping of flexural beam vibrations. Journal of Sound and Vibration. 2019;450:28-46.
[33] Mironov MA, Pislyakov VV. One-dimensional acoustic waves in retarding structures with propagation velocity tending to zero. Acoustical Physics. 2002;48:347–52.
[34] Wang X, Wang J, Chen Y. Research on Ultrabroadband Acoustic Absorbers Based on Slow-wave Metamaterials. 2021 OES China Ocean Acoustics (COA)2021. p. 219-23.
[35] Guasch O, Arnela M, Sánchez-Martín P. Transfer matrices to characterize linear and quadratic acoustic black holes in duct terminations. Journal of Sound and Vibration. 2017;395:65-79.
[36] Hollkamp JP, Semperlotti F. Application of fractional order operators to the simulation of ducts with acoustic black hole terminations. Journal of Sound and Vibration. 2020;465.
[37] Yang J, Lee JS, Kim YY. Multiple slow waves in metaporous layers for broadband sound absorption. Journal of Physics D: Applied Physics. 2017;50.

[38] Bonatti C, Mohr D. Smooth-shell metamaterials of cubic symmetry: Anisotropic elasticity, yield strength and specific energy absorption. Acta Materialia. 2019;164:301-21.
[39] Li X, Tan YH, Willy HJ, Wang P, Lu W, Cagirici M, et al. Heterogeneously tempered martensitic high strength steel by selective laser melting and its micro-lattice: Processing, microstructure, superior performance and mechanisms. Materials & Design. 2019;178:107881.
[40] Wang D. Sound absorption of face-centered cubic sandwich structure with micro-perforations. Materials and Design. 2020:10.
[41] Deshmukh S, Ronge H, Ramamoorthy S. Design of periodic foam structures for acoustic applications: Concept, parametric study and experimental validation. Materials & Design. 2019;175.
[42] Li X, Yu X, Zhai W. Additively Manufactured Deformation-Recoverable and Broadband Sound-Absorbing Microlattice Inspired by the Concept of Traditional Perforated Panels. Adv Mater. 2021;33:e2104552.
[43] Chua JW, Li X, Li T, Chua BW, Yu X, Zhai W. Customisable sound absorption properties of functionally graded metallic foams. Journal of Materials Science & Technology. 2022;108:196-207.
[44] Fotsing ER, Dubourg A, Ross A, Mardjono J. Acoustic properties of periodic micro-structures obtained by additive manufacturing. Applied Acoustics. 2019;148:322-31.
[45] Boulvert J, Costa-Baptista J, Cavalieri T, Perna M, Fotsing ER, Romero-García V, et al. Acoustic modeling of micro-lattices obtained by additive manufacturing. Applied Acoustics. 2020;164.
[46] Bilal OR, Ballagi D, Daraio C. Architected Lattices for Simultaneous Broadband Attenuation of Airborne Sound and Mechanical Vibrations in All Directions. Physical Review Applied. 2018;10.